

Two loop virtual corrections to $b \rightarrow (d, s)\ell^+\ell^-$ and $c \rightarrow u\ell^+\ell^-$ for arbitrary momentum transfer

STEFAN DE BOER^a

^a*Fakultät für Physik,
TU Dortmund, Otto-Hahn-Str.4, 44221 Dortmund, Germany*

Abstract

Non-factorizable two loop corrections to heavy to light flavor changing neutral current transitions due to matrix elements of current-current operators are calculated analytically for arbitrary momentum transfer. This extends previous works on $b \rightarrow (d, s)\ell^+\ell^-$ transitions. New results for $c \rightarrow u\ell^+\ell^-$ transitions are presented. Recent works on polylogarithms are used for the master integrals. For $b \rightarrow s\ell^+\ell^-$ transitions, the corrections are most significant for the imaginary parts of the effective Wilson coefficients in the large hadronic recoil range. Analytical results and ready-to-use fitted results for a specific set of parameters are provided.

1 Introduction

Recently, several discrepancies with the standard model (SM) have been revealed in $b \rightarrow s\ell^+\ell^-$ induced decays, e.g., [1]. However, those that do not involve lepton flavor universality violation are not definitely settled due to poorly controlled non-perturbative effects of quantum chromodynamics (QCD). Exemplary, non-factorizable corrections to form factors are commonly considered as one unreducible uncertainty while interpreting beyond the standard model (BSM) physics. Furthermore, in $c \rightarrow u\ell^+\ell^-$ transitions, non-factorizable corrections yield the largest perturbative contribution due to the Glashow–Iliopolus–Maiani (GIM) cancellation of factorizable contributions [2–4]. In this paper, we improve on the current state by calculating the two loop virtual corrections to any heavy to light transition, including c and b decays, induced by current-current operators for arbitrary invariant dilepton mass q^2 .

Partonic transitions are a first approximation to the corresponding inclusive hadronic decays in the framework of an operator product expansion (OPE). This approximation is applicable away from resonance regions and up to power corrections. The resonance regions can be handled by appropriate kinematical cuts and power corrections can be treated within a heavy quark expansion (an expansion in inverse powers of the heavy quark mass, see [5] for $b \rightarrow s$ transitions). Furthermore, perturbative results are the basis for estimates of non-perturbative effects in inclusive and exclusive hadronic decays, e.g., [6, 7].

Several calculations were performed for $b \rightarrow (d, s)$ transitions: In [8] and [9] $b \rightarrow s$ and $b \rightarrow d$ transitions, respectively, were computed for small q^2 . The calculation of $b \rightarrow s$ transitions for large q^2 was accomplished in [10]. A seminumerical approach was employed in [5] to present results based on $b \rightarrow s$ transitions for the full q^2 range. In [11] $b \rightarrow d$ transitions for any q^2 range were computed, extending [9]. For $c \rightarrow u$ transitions, see [12]. We emphasize that available results for $b \rightarrow (d, s)$ transitions only cover different limits, i.e. zero masses, small and large q^2 ranges, and that results for $c \rightarrow u$ transitions have become available only recently [4, 12]. The analytic calculation presented in this paper covers the full q^2 range, arbitrary masses and electric charges.

Generally, the effective weak Lagrangian for heavy to light quark flavor changing neutral current (FCNC) transitions $h \rightarrow l$ at the low-energy scale μ is written as

$$\mathcal{L}_{\text{eff}} = \frac{4G_F}{\sqrt{2}} \sum_q \lambda_q \left(C_1 P_1^{(q)} + C_2 P_2^{(q)} + \sum_{i=3}^{10} C_i P_i \right), \quad (1)$$

where the sum is over light quark fields q with masses below μ , and products of Cabibbo–Kobayashi–Maskawa (CKM) matrix elements $\lambda_q = V_{q(d,s)}^* V_{qb}, V_{cq}^* V_{uq}$ for $b \rightarrow (d, s)$ and $c \rightarrow u$ transitions, respectively. Here, C_i are the Wilson coefficients and the physical

operators P_i , which are relevant for this paper, read

$$P_1^{(q)} = (\bar{l}_L \gamma_{\mu_1} T^a q_L)(\bar{q}_L \gamma^{\mu_1} T^a h_L), \quad (2)$$

$$P_2^{(q)} = (\bar{l}_L \gamma_{\mu_1} q_L)(\bar{q}_L \gamma^{\mu_1} h_L), \quad (3)$$

$$P_7 = \frac{e}{g_s^2} m_h (\bar{l}_L \sigma^{\mu_1 \mu_2} h_R) F_{\mu_1 \mu_2}, \quad (4)$$

$$P_9 = \frac{e^2}{g_s^2} (\bar{l}_L \gamma_{\mu_1} h_L)(\bar{\ell} \gamma^{\mu_1} \ell), \quad (5)$$

where $q_{L/R} = \frac{1}{2}(1 \mp \gamma_5)q$, $\sigma^{\mu_1 \mu_2} = \frac{i}{2}[\gamma^{\mu_1}, \gamma^{\mu_2}]$, and T^a are the $SU(3)_C$ generators normalized to $\text{Tr}[T^a T^b] = \frac{\delta^{ab}}{2}$. Furthermore, G_F is the Fermi constant, $F_{\mu_1 \mu_2}$ denotes the electromagnetic field strength tensor, and g_s and e are the strong and electromagnetic coupling constants, respectively.

We calculate the two loop QCD matrix elements of $P_{1/2}$, in terms of form factors (i.e., for inclusive decays, effective Wilson coefficients) multiplying the matrix elements of $P_{7,9}$, for $h \rightarrow \ell \ell^+ \ell^-$ transitions. The result is valid for a general class of heavy to light transitions with arbitrary invariant momentum transfer and masses, when the mass of the light quark is neglected. This includes the transitions $b \rightarrow (d, s)$ via $(u\bar{u}, c\bar{c})$ loops, and $c \rightarrow u$ via $(d\bar{d}, s\bar{s})$ loops, where the loop quark-antiquark pair $(q\bar{q})$ is annihilated and a photon is emitted, which may then couple to a lepton pair. Note that the computation of two loop matrix elements presented in this paper is not restricted to SM applications, see [12] for an example in leptoquark models. We use the recent works [13] and [14] for the master integrals (MIs) and their numerical evaluation, respectively.

We outline our calculation in the section 2, see also [12]. The numerical evaluation is detailed in section 2.1. Results are given in section 3, where we also comment on the phenomenological impact for $b \rightarrow (d, s)$ transitions. For the phenomenology of $c \rightarrow u$ transitions, see [12]. Appendix A contains a description of supplemented files, which encode the results of this paper.

2 Outline of the calculation

In this section, we outline the calculation of the diagrams shown in figure 1. Each of the five subsets represents a gauge invariant class. A sixth class, shown in figure 2, preserves the operator structure of P_9 , hence it is commonly considered as a correction to the matrix element of P_9 [8] and not included in the calculation presented in this paper. Nevertheless, we have checked that in this class only the diagram with a photon coupling to the loop of the quark-antiquark pair is non-zero and factorizes into two one loop integrals. It is the only diagram with infrared and collinear singularities.

We calculate the diagrams in figure 1 with insertions of P_2 . Insertions of P_1 are then given by color factors due to additional generators in the definition of the operator: The expressions for the first four and last (two) classes are multiplied with $-\frac{1}{6}$ and $\frac{4}{3}$, respectively.

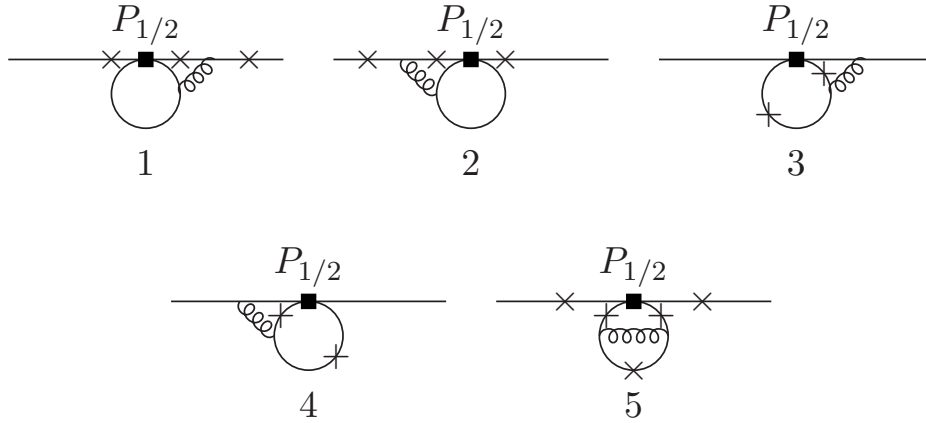


Figure 1: Diagrams for heavy to light quark transitions at two loop QCD. The boxes denote operator insertions of $P_{1/2}$. The crosses indicate the emission of a photon, which may then couple to a lepton pair.

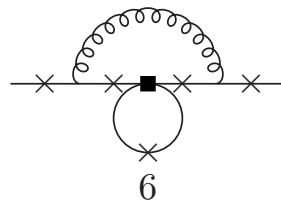


Figure 2: A sixth class of diagrams, see figure 1 and text.

The matrix element for an off-shell photon γ^* can be decomposed as [11]

$$\begin{aligned}
\langle \gamma^*(q, \mu) l(p_l) | P_2 | h(p_h) \rangle &= \langle l(p_l) | \bar{l} X^\mu h | h(p_h) \rangle \\
&= \left(\frac{\alpha_s}{4\pi} \right)^2 F^{(q)}(q^2) \langle l(p_l) | \bar{l}_L q^\mu h_L | h(p_h) \rangle \\
&+ \left(\frac{\alpha_s}{4\pi} \right)^2 F^{(7)}(q^2) \langle l(p_l) | \bar{l}_L \sigma^{\mu\nu} q_\nu h_R | h(p_h) \rangle \\
&+ \left(\frac{\alpha_s}{4\pi} \right)^2 F^{(9)}(q^2) \langle l(p_l) | \bar{l}_L (q^2 \gamma^\mu - q^\mu \not{q}) h_L | h(p_h) \rangle, \quad (6)
\end{aligned}$$

where $q^\mu = (p_h - p_l)^\mu$ is the transferred momentum, and X^μ is the sum of the amputated diagrams in figure 1.

The scalar form factors $F^{(i)}$ are given as [11]

$$F^{(i)}(q^2) = \text{Tr}[P_i^\mu X_\mu] \quad (7)$$

with the projectors

$$P_i^\mu = (\not{p}_h + m_h)(C_{i1}q^\mu + C_{i2}p_h^\mu + C_{i3}\gamma^\mu)\not{p}_l \quad (8)$$

and coefficients C_{ij} . The factors $(\not{p}_h + m_h)$ and \not{p}_l reflect the on-shell conditions for the external quarks. The form factors for $\langle l\bar{l}l | P_2 | h \rangle$, thus the effective Wilson coefficients, are proportional to $F^{(7,9)}$. By gauge invariance, the form factor $F^{(q)}$ vanishes for each class, which we have checked.

For the calculation, we utilize the computer programs **FORM 4.0** [15] and **REDUZE 2** [16]. We use the former for algebraic manipulations, e.g. the tensor algebra, and the latter is used for the reduction to MIs. The program **REDUZE 2** is based on the Laporta algorithm [17] which employs integration by parts (IBP) identities [18] and Lorentz invariance (LI) identities [19]. Indeed, LI identities can be written as linear combinations of IBP identities [20]. We have calculated relations for each diagram based on LI identities by hand and checked them against the reduction tables built with **REDUZE 2**.

We find that the following diagrams in figure 1 vanish: In the fifth class, both diagrams with photons attached to the external lines vanish. The diagram with a photon emitted from the heavy quark line in the first class is zero. For $F^{(7)}$, all diagrams with photons attached to the external lines vanish. Furthermore, all diagrams of the fifth class vanish for $F^{(7)}$. This implies that the $\langle P_1 \rangle$ induced dipole form factor is given by $\frac{-1}{6} F^{(7)}$.

As for the set of the MIs, we match a subset of the integrals calculated in [13]. A canonical set is given in [10], where the MIs are calculated for large q^2 , yet the set of integrals is not minimal. While matching the set of [10] onto the MIs taken from [13], we find additional relations among the former, e.g. for the integral I_{d23} and the one of equation (A12) in [10]. Furthermore, we do not encounter the integrals of equations (A5), (A8), and (A14) in [10].

With the MIs from [13] the unrenormalized form factors are expressed in terms of (generalized) harmonic polylogarithms (HPLs), see the next section for the numerical

evaluation. The prescription for the renormalization is described in, e.g., [8]. Accordingly, the operator renormalization constants are written as

$$Z_{ij} = \delta_{ij} + \delta Z_{ij},$$

$$\delta Z_{ij} = \frac{\alpha_s}{4\pi} \left(a_{ij}^{01} + \frac{1}{\epsilon} a_{ij}^{11} \right) + \frac{\alpha_s^2}{(4\pi)^2} \left(a_{ij}^{02} + \frac{1}{\epsilon} a_{ij}^{12} + \frac{1}{\epsilon^2} a_{ij}^{22} \right) + \mathcal{O}(\alpha_s^3), \quad (9)$$

where the dimension is $4 - 2\epsilon$. Extending the set of the physical operators P_i by the evanescent operators $E_{11,12}$ defined as

$$E_{11} = (\bar{l}_L \gamma_{\mu_1} \gamma_{\mu_2} \gamma_{\mu_3} T^a q_L) (\bar{q}_L \gamma^{\mu_1} \gamma^{\mu_2} \gamma^{\mu_3} T^a h_L) - 16P_1, \quad (10)$$

$$E_{12} = (\bar{l}_L \gamma_{\mu_1} \gamma_{\mu_2} \gamma_{\mu_3} q_L) (\bar{q}_L \gamma^{\mu_1} \gamma^{\mu_2} \gamma^{\mu_3} h_L) - 16P_2. \quad (11)$$

the coefficients a_{ij} are compactly written as

$$a^{11}|_{i=1,2} = \begin{pmatrix} -2 & \frac{4}{3} & 0 & -\frac{1}{9} & 0 & 0 & 0 & 0 & -\frac{8}{9}q_i & 0 & \frac{5}{12} & \frac{2}{9} \\ 6 & 0 & 0 & \frac{2}{3} & 0 & 0 & 0 & 0 & -\frac{2}{3}q_i & 0 & 1 & 0 \end{pmatrix}, \quad (12)$$

and

$$-6 a_{17}^{12} = a_{27}^{12} = 2q_i - \frac{8}{27}q_e, \quad a_{19}^{12} = -\frac{2}{9}q_i - \frac{44}{243}q_e, \quad a_{29}^{12} = \frac{16}{3}q_i + \frac{88}{81}q_e, \quad (13)$$

$$a_{19}^{22} = \frac{92}{9}q_i - \frac{16}{27}n_f q_i + \frac{8}{81}q_e, \quad a_{29}^{22} = \frac{14}{3}q_i - \frac{4}{9}n_f q_i - \frac{16}{27}q_e. \quad (14)$$

Here, $P_4 = (\bar{l}_L \gamma_{\mu_1} T^a h_L) \sum_{\{q:m_q < \mu\}} (\bar{q} \gamma^{\mu_1} T^a q)$, n_f is the number of flavors and $q_{e,i}$ are the charges of the external and internal quarks, respectively, i.e. $q_e = \frac{-1}{3}$, $q_i = \frac{2}{3}$ for $b \rightarrow (d, s)$ and $q_e = \frac{2}{3}$, $q_i = \frac{-1}{3}$ for $c \rightarrow u$ transitions. The coefficients $a_{ij}^{11,22}$ can be obtained from the leading order (LO) anomalous dimension matrix (ADM) $\gamma^{(0)}$ and the coefficients a_{ij}^{12} from [21],

$$a^{11} = \frac{1}{2}\gamma^{(0)}, \quad a^{12} = \frac{1}{4}\gamma^{(1)} + \frac{1}{2}\hat{b} \cdot \hat{c}, \quad a^{22} = \frac{1}{8}\gamma^{(0)} \cdot \gamma^{(0)} - \frac{1}{4}\beta_0\gamma^{(0)}, \quad (15)$$

where $\gamma^{(1)}$ is the next-to leading order (NLO) ADM, and the mixing via the evanescent operators is found as

$$\hat{b}|_{i=1,2} = \begin{pmatrix} \frac{5}{12} & \frac{2}{9} \\ 1 & 0 \end{pmatrix}, \quad \hat{c}|_{j=9} = \begin{pmatrix} \frac{32}{9}q_i \\ \frac{8}{3}q_i \end{pmatrix}. \quad (16)$$

The counterterm form factors $F_{i \rightarrow (7,9)}^{\text{ct}(7,9)}$, due to the mixing of $P_{1/2}$ into $P_{7,9}$, and the one loop renormalization of g_s in the definition of P_9 , are [8, 9]

$$F_{i \rightarrow 7}^{\text{ct}(7)} = -\frac{a_{i7}^{12}}{\epsilon}, \quad F_{i \rightarrow 9}^{\text{ct}(9)} = -\left(\frac{a_{i9}^{22}}{\epsilon^2} + \frac{a_{i9}^{12}}{\epsilon} \right) - \frac{a_{i9}^{11}\beta_0}{\epsilon^2}, \quad (17)$$

where $\beta_0 = 11 - \frac{2}{3}n_f$.

The counterterms $F_{i \rightarrow 4\text{quark}}^{\text{ct}(7,9)}$, due to the mixing of $P_{1/2}$ into four-quark operators P_j , are defined by [8]

$$\sum_j \frac{\alpha_s}{4\pi} \frac{1}{\epsilon} a_{ij}^{11} \langle l\ell\ell | P_j | h \rangle_{1\text{loop}} = - \left(\frac{\alpha_s}{4\pi} \right)^2 \left(F_{i \rightarrow 4\text{quark}}^{\text{ct}(7)} \langle P_7 \rangle_{\text{tree}} + F_{i \rightarrow 4\text{quark}}^{\text{ct}(9)} \langle P_9 \rangle_{\text{tree}} \right). \quad (18)$$

We calculate them to $\mathcal{O}(\epsilon)$ and for insertions of $P_{1,2,4}$, $E_{11,12}$ according to eqs. (18) and (12), respectively. We write

$$I(m_q^2) = \left(\frac{\mu^2}{m_q^2} \right)^\epsilon \int_0^1 dz (1-z) z \left(-\frac{6}{\epsilon} + 6 - 6 \ln \frac{1}{1-z(1-z)q^2/m_q^2} - \frac{\pi^2}{2} \epsilon \right. \\ \left. + 6\epsilon \ln \frac{1}{1-z(1-z)q^2/m_q^2} - 3\epsilon \ln^2 \frac{1}{1-z(1-z)q^2/m_q^2} \right), \quad (19)$$

where in the massless limit, $m_q^2 \rightarrow 0$,

$$\int_0^1 dz (1-z) z \ln \frac{1}{1-z(1-z)q^2/m_q^2} \rightarrow \frac{5}{18} - \frac{1}{6} \ln \frac{q^2}{m_q^2} + i\frac{\pi}{6}, \\ \int_0^1 dz (1-z) z \ln^2 \frac{1}{1-z(1-z)q^2/m_q^2} \rightarrow \frac{28}{27} + i\frac{5\pi}{9} - \frac{2\pi^2}{9} - \frac{5}{9} \ln \frac{q^2}{m_q^2} - i\frac{\pi}{3} \ln \frac{q^2}{m_q^2} \\ + \frac{1}{6} \ln^2 \frac{q^2}{m_q^2}, \quad (20)$$

and the residual m_q^2 dependence cancels to $\mathcal{O}(\epsilon)$ in eq. (19). With this, the matrix elements are evaluated to

$$\langle l\ell\ell | P_1 | h \rangle_{1\text{loop}} = -\frac{8}{9} q_i I(m_q^2) \frac{\alpha_s}{4\pi} \langle P_9 \rangle_{\text{tree}}, \\ \langle l\ell\ell | P_2 | h \rangle_{1\text{loop}} = \frac{3}{4} \langle l\ell\ell | P_1 | h \rangle_{1\text{loop}}, \\ \langle l\ell\ell | P_4 | h \rangle_{1\text{loop}} = -\frac{4}{3} q_e \left(\frac{\mu^2}{m_c^2} \right)^\epsilon \left(-1 - \epsilon \int_0^1 dz \ln \frac{1}{1-z(1-z)q^2/m_c^2} \right) \frac{\alpha_s}{4\pi} \langle P_7 \rangle_{\text{tree}} \\ - \frac{8}{9} q_e (I(m_c^2) + I(0)) \frac{\alpha_s}{4\pi} \langle P_9 \rangle_{\text{tree}}, \\ \langle l\ell\ell | E_{11} | h \rangle_{1\text{loop}} = -4 \left(-\frac{8}{9} q_i \right) \left(\frac{\mu^2}{m_q^2} \right)^\epsilon \int_0^1 dz (1-z) z \left(-6 - 6\epsilon \ln \frac{1}{1-z(1-z)q^2/m_q^2} \right) \\ \times \frac{\alpha_s}{4\pi} \langle P_9 \rangle_{\text{tree}}, \\ \langle l\ell\ell | E_{12} | h \rangle_{1\text{loop}} = \frac{3}{4} \langle l\ell\ell | E_{11} | h \rangle_{1\text{loop}}. \quad (21)$$

We have checked that expanding the matrix elements in small q^2 and in the limit $m_q^2 \rightarrow 0$ yields the results in [8] and [11], respectively.

Following [8], the renormalization of the mass m_q is given by the replacement $m_q \rightarrow Z_m m_q$ in $\langle l\ell\ell|P_{1,2}|h\rangle_{\text{loop}}$ of eq. (21). The mass renormalization constants Z_m in the modified minimal subtraction ($\overline{\text{MS}}$) and the pole mass scheme are [22]

$$\begin{aligned} Z_m^{\overline{\text{MS}}} &= 1 + \frac{\alpha_s}{4\pi} \left(-\frac{4}{\epsilon} \right) + \mathcal{O}(\alpha_s^2), \\ Z_m^{\text{pole}} &= 1 + \frac{\alpha_s}{4\pi} \left(-\frac{4}{\epsilon} - 4 \ln \frac{\mu^2}{m^2} - \frac{16}{3} \right) + \mathcal{O}(\alpha_s^2). \end{aligned} \quad (22)$$

Expanding the matrix elements at $\mathcal{O}(\frac{\alpha_s}{4\pi})$ and $\mathcal{O}(\epsilon^0)$ gives the counterterms $F_{i,m_q}^{\text{ct}(9)}$ and $F_{i,m_q}^{\text{ct}(7)} = 0$. We have checked for both schemes that expanding the counterterm $F_{i,m_q}^{\text{ct}(9)}$ in small q^2 yields the results in [8].

Factorizable form factors represented by class 5 in figure 1 are found to be renormalized separately by the mass renormalization and mixing into evanescent operators, i.e. $a_{211}^{11} = \frac{1}{2}$ in eq. (12), and $a_{29}^{12} = \frac{4}{9}q_i$ in eq. (13) are the only non-zero coefficients for the counterterms of $F_2^{(9fac)}$; recall that the $\langle P_1 \rangle$ induced factorized form factor is given by color factors and the dipole factorized form factors are zero.

Finally, the renormalized form factors are given by subtracting $F_i^{\text{ct}(7,9)} = (F_{i \rightarrow 7,9}^{\text{ct}(7,9)} + F_{i \rightarrow 4\text{quark}}^{\text{ct}(7,9)} + F_{i,m_q}^{\text{ct}(7,9)})$ from the unrenormalized form factors. Note that wave function renormalization of the external quark fields would need to be taken into account only if we wanted to include the diagrams of figure 2 [8]. We have checked that $F_i^{\text{ct}(7)}|_{\epsilon^0}$ agrees with the results in [5].

2.1 Numerical evaluation

The analytical results for the renormalized form factors as found in the previous section are provided as supplemented files, see appendix A. In this section, we describe the numerical evaluation of the MIs [13], which are expressed in terms of HPLs. Note that the undetermined $\tilde{M}_{19}|_{\epsilon^4}$ [13] in the MIs cancels in the form factors. In accordance with [13], we choose the analytical continuation by subtracting from the internal mass an infinitesimal imaginary part $\eta > 0$, i.e. $m_i^2 \rightarrow m_i^2 - i\eta$. For negative invariant momentum transfer, an infinitesimal imaginary part is subtracted from q^2 , and $m_i^2 \rightarrow m_i^2 + i\eta$. Note that for positive invariant momentum transfer the addition of an infinitesimal imaginary part to q^2 is not necessary, i.e. real q^2 can be chosen. For the evaluation of the factorizable results, we find that real q^2 are sufficient for any momentum transfer. We write the HPLs as generalized/Goncharov polylogarithms (GPLs), see, e.g., [13] (and references therein) and feed them into the computer package `lieevaluate` [14]. Other packages for the numerical evaluation of GPLs can be found in [23, 24].

While evaluating the expressions with `lieevaluate`, we encounter the undefined function $\theta(0)$ and the function `MyP` [14] that is divergent for some arguments of GPLs [14]. We regulate the former by a perturbation of these arguments, see [14]. We have numerically checked that the form factors are insensitive to the actual choice of such

perturbations. The divergences due to the function `MyP` cancel in the form factors within the numerical precision.

We have checked that the numerical evaluation of the MIs with `lieevaluate` yields a precision better than 10^{-6} with respect to [13].¹ Moreover, numerical agreement of the MIs in terms of HPLs is found by use of the package `HypExp 2` [25, 26] and also via numerical integration within `Mathematica`, yet the convergence is partially slow.

The analytical expressions are lengthy and their numerical evaluation is involved. Hence, we evaluate the form factors for fixed mass parameters and at different q^2 points. Note that the numerical evaluation close to the kinematical endpoints $q^2 = 0, m_h^2$ is sensitive to the ratio of mass parameters and q^2 . Finally, we fit the points.

Subtracting the counterterm form factors from the unrenormalized form factors, the $\frac{1}{\epsilon^2}$ and $\frac{1}{\epsilon}$ divergences cancel numerically. We have checked our calculation against the ones of [8, 10, 11] for $b \rightarrow (d, s)$ transitions, finding numerical agreement for different q^2 , scales, mass schemes, and parameters, see the next section. For $c \rightarrow u\gamma$ transitions, the effective dipole Wilson coefficient at $q^2 = 0$ induced by $\langle P_2 \rangle$ was calculated in [2]. Adding the constant terms given in [3] we have checked the calculations, finding numerical agreement.

3 Results

Our fitted results of the renormalized form factors $F_{1,2}^{(7,9)}$ induced by $\langle l\ell l | P_{1,2} | h \rangle$ for $b \rightarrow (d, s)$ and $c \rightarrow u$ transitions are shown in figures 3-6 for $q^2 \in [0, m_h^2]$. For comparison, we also show the results of [8, 10, 11]. We use the (pole) masses

$$m_b = 4.85 \text{ GeV}, \quad m_c = 1.47 \text{ GeV}, \quad m_s = 0.13 \text{ GeV}, \quad (23)$$

$m_{u,d} \approx 0$ and set $\mu = m_h$ if not stated otherwise.

We note the following:

- The results of [8, 10, 11] agree well with our results, hence the former are only partially visible in the plots.
- The form factors are divergent at the internal quark pair mass squared $q^2 = (2m_i)^2$.
- The lower left plot of figure 3 indicates a numerical precision of our results better than 10^{-3} with respect to the analytical result of [11].
- The lower right plot of figure 3 shows agreement with the expansion of [10] at high q^2 . Note that we do not plot the ratio close to the kinematical endpoint $q^2 = m_b^2$, where the evaluation of the result of [10] yields oscillations. At low q^2 , a breakdown of the convergence of the expansion of [8] is visible around $q^2 \sim 5 \text{ GeV}^2$, where the sensitivity on μ increases. Similar conclusions are drawn from figure 5.

Furthermore, note that our definition of the form factors and the one in [8, 10] differs by a minus sign. Recall that $F_1^{(7)} = \frac{-1}{6} F_2^{(7)}$. For $F_{1,2}^{(9)}$, the numerical precision of our results is better than 10^{-2} with respect to the results of [8, 10, 11] for $b \rightarrow (d, s)$ transitions.

¹We acknowledge the authors of [13] for providing additional code on their work.

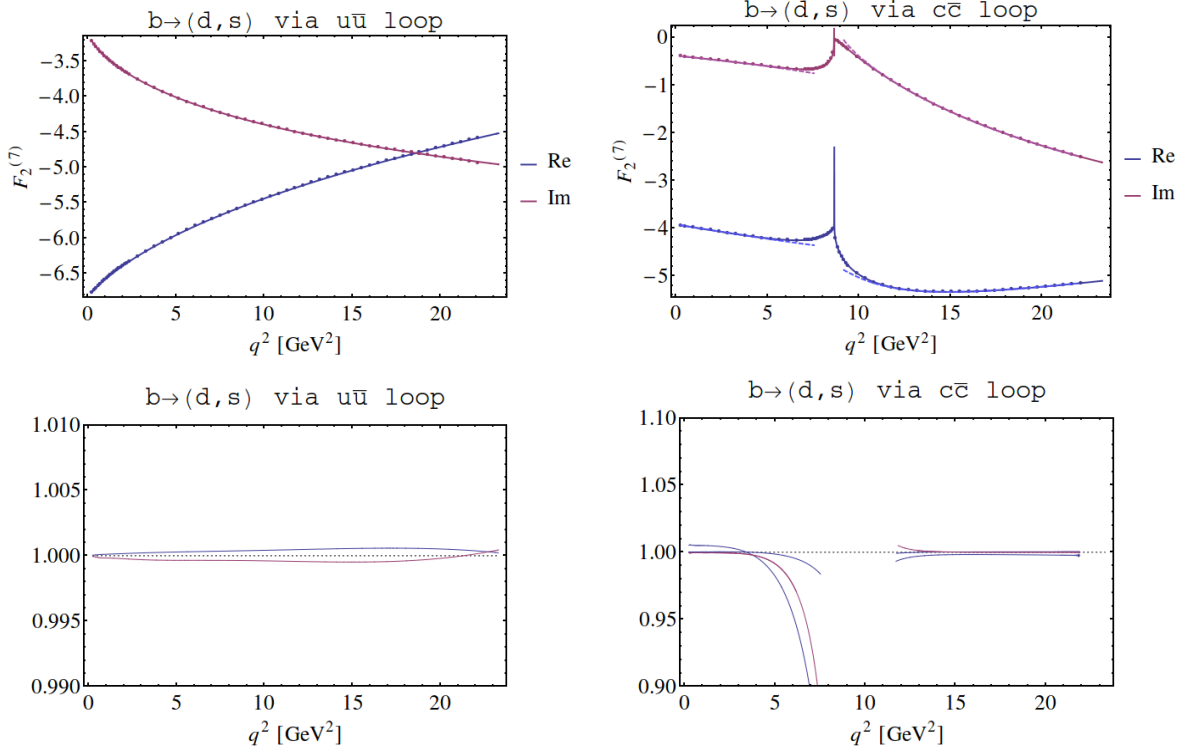


Figure 3: Real (blue) and imaginary (purple) parts of the form factor $F_2^{(7)}$ induced by $\langle P_2^{(u)} \rangle$ (left) and $\langle P_2^{(c)} \rangle$ (right) for $b \rightarrow (d, s)$ transitions. The solid lines are fitted to the points, which represent the results of the numerical evaluation. The dashed lines show the expansions of [8, 10], whereas, in the upper left plot, the result of [11] agrees with the solid lines. The lower plots show the ratio of the fitted curves with respect to results of [11] (lower left) and the expansions of [8, 10] (lower right), where $\mu = \frac{1}{2}m_b, 2m_b$. A ratio of one is indicated by the black dotted line in the lower plots.

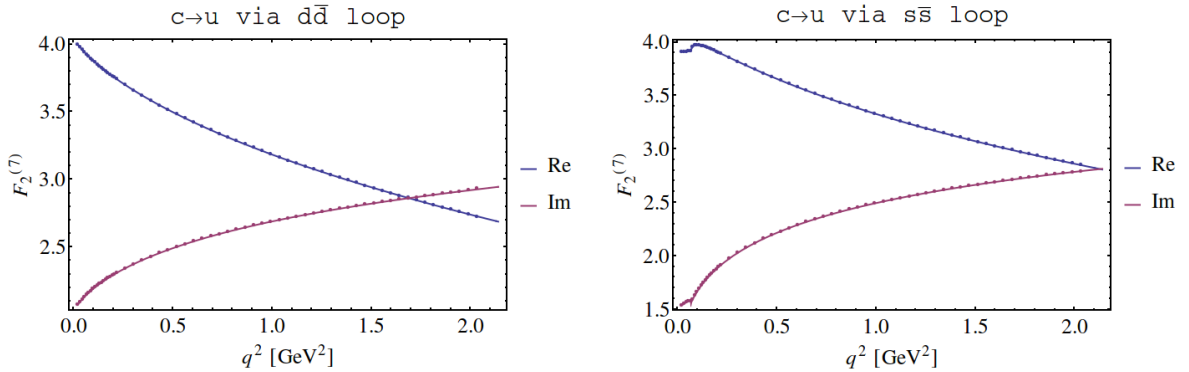


Figure 4: Real (blue) and imaginary (purple) parts of the form factor $F_2^{(7)}$ induced by $\langle P_2^{(d)} \rangle$ (left) and $\langle P_2^{(s)} \rangle$ (right) for $c \rightarrow u$ transitions. The solid lines are fitted to the points, which represent the results of the numerical evaluation.

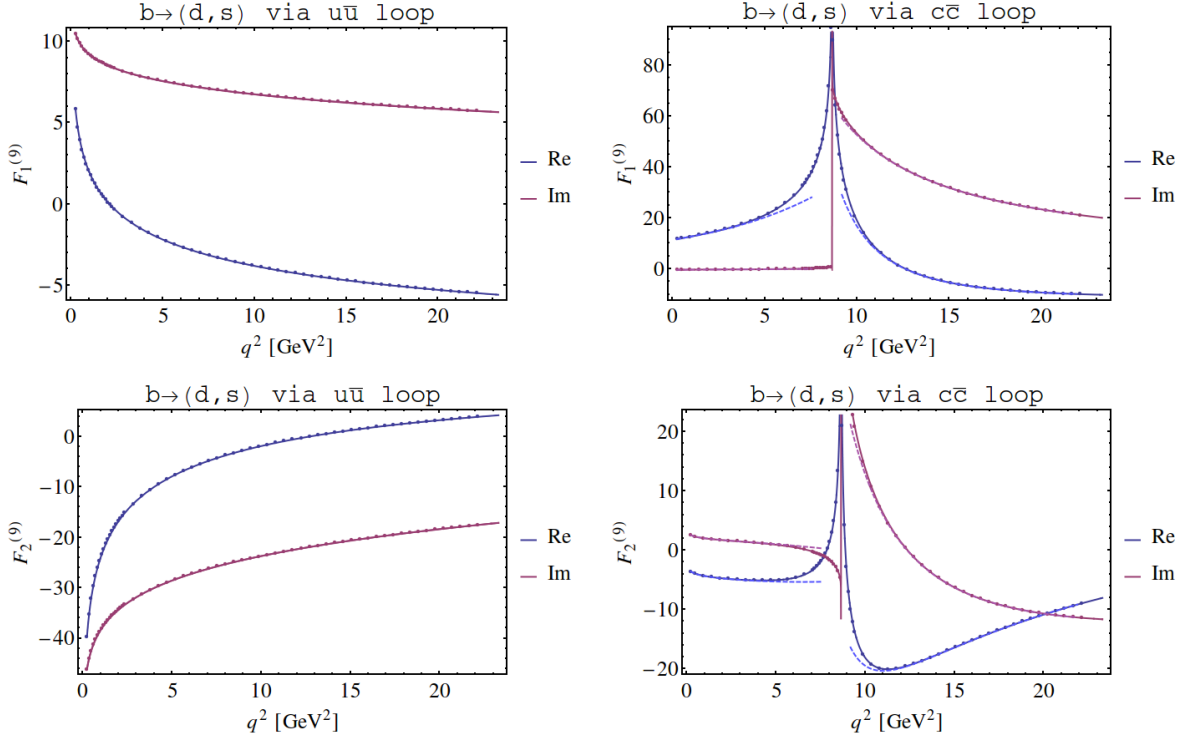


Figure 5: Real (blue) and imaginary (purple) parts of the form factor $F_{1,2}^{(9)}$ induced by $\langle P_1^{(u)} \rangle$ (upper left), $\langle P_1^{(c)} \rangle$ (upper right), $\langle P_2^{(u)} \rangle$ (lower left), and $\langle P_2^{(c)} \rangle$ (lower right) for $b \rightarrow (d, s)$ transitions. The solid lines are fitted to the points, which represent the results of the numerical evaluation. The dashed lines show the expansions of [8, 10], whereas, in the left plots, the results of [11] agree with the solid lines.

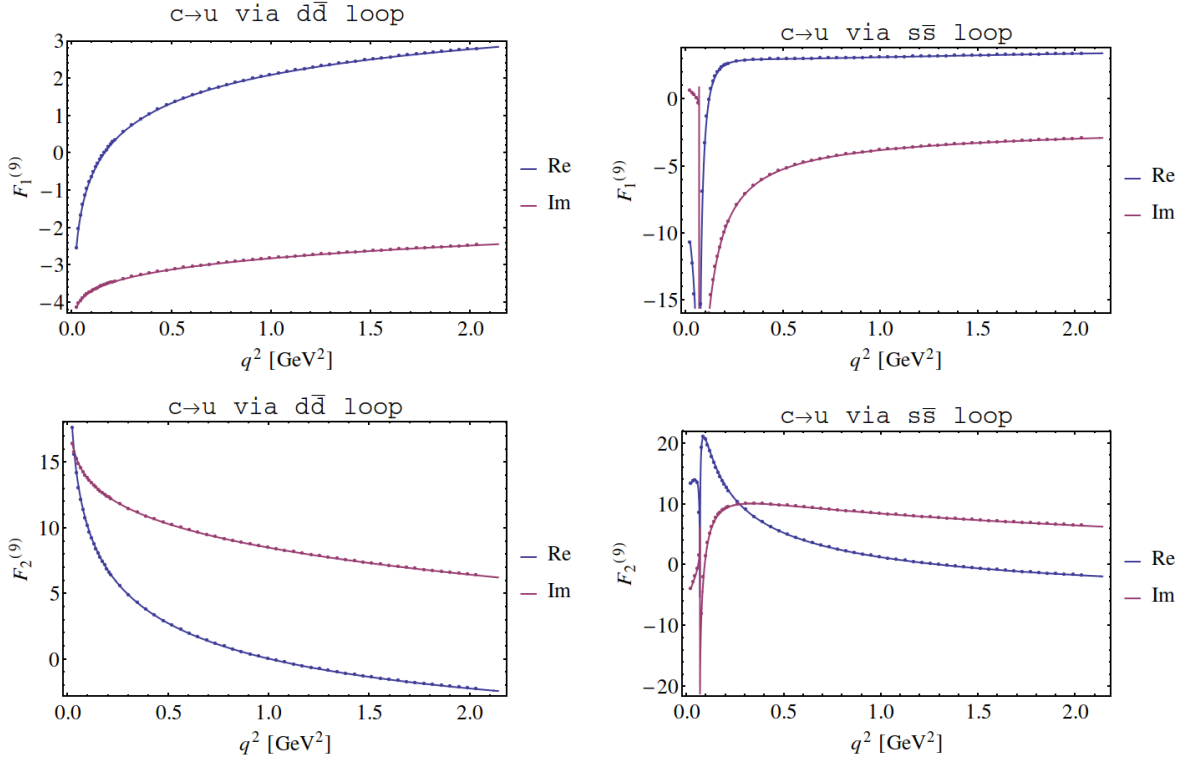


Figure 6: Real (blue) and imaginary (purple) parts of the form factor $F_{1,2}^{(9)}$ induced by $\langle P_1^{(d)} \rangle$ (upper left), $\langle P_1^{(s)} \rangle$ (upper right), $\langle P_2^{(d)} \rangle$ (lower left), and $\langle P_2^{(s)} \rangle$ (lower right) for $c \rightarrow u$ transitions. The solid lines are fitted to the points, which represent the results of the numerical evaluation.

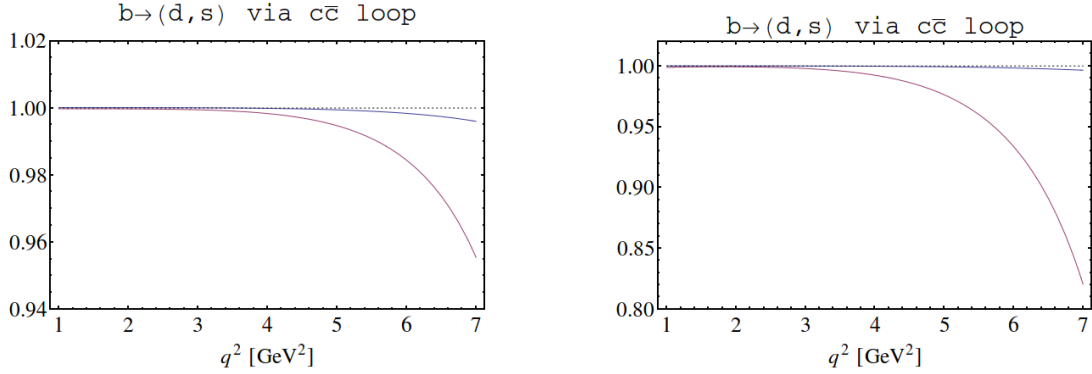


Figure 7: Ratios $\frac{\text{Re}[\tilde{C}_7^{\text{eff}}]_{\text{this}}}{\text{Re}[\tilde{C}_7^{\text{eff}}]_{[8]}}$ (blue) and $\frac{\text{Im}[\tilde{C}_9^{\text{eff}}]_{\text{this}}}{\text{Im}[\tilde{C}_9^{\text{eff}}]_{[8]}}$ (purple) of the effective Wilson coefficients \tilde{C}_7^{eff} (left) and \tilde{C}_9^{eff} (right) for $b \rightarrow (d, s)$ transitions induced by a massive internal charm quark. We follow [5, 10], adding the results of this paper and the expansion of [8] for $\mu = 5 \text{ GeV}$. A ratio of one is indicated by the black dotted line.

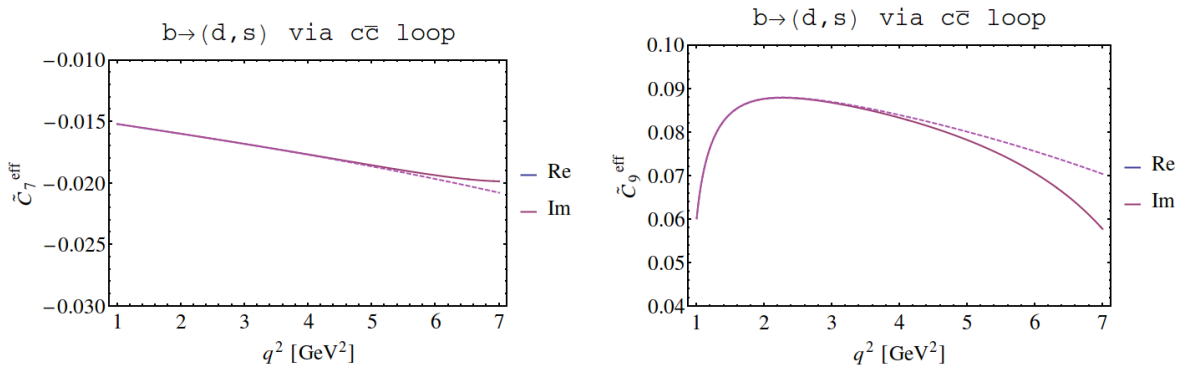


Figure 8: Imaginary parts of the effective Wilson coefficients \tilde{C}_7^{eff} (left) and \tilde{C}_9^{eff} (right) for $b \rightarrow (d, s)$ transitions induced by a massive internal charm quark. We follow [5, 10], adding the results of this paper (solid) and the expansion of [8] (dashed) for $\mu = 5 \text{ GeV}$.

We deduce that the overall numerical precision of our result is better than a percent. To have ready-to-use result at hand, we provide our results for the masses of eq. (23) as supplemented files, see appendix A.

Next, we comment on the impact of the new results for $b \rightarrow (d, s)$ transitions. For massless internal quarks an independent analytical result is provided in [11]. The high q^2 range for massive internal quarks is well approximated by the results of [10]. On the other side, compared to the low q^2 range [8] for massive internal quarks, our results indicate significant corrections around $q^2 \sim 5 \text{ GeV}^2$. Following [5] and [10] for the matrix element of the chromomagnetic operator, the effective Wilson coefficients $\tilde{C}_{7,9}^{\text{eff}}$ at next-to-next-to leading logarithmic (NNLL) order are shown in figures 7, 8. We add our results and, for comparison, the results of [8] for $1 \text{ GeV}^2 \leq q^2 \leq 7 \text{ GeV}^2$. Note that for phenomenological purposes $\tilde{P}_{7,9} = \frac{\alpha_s}{4\pi} P_{7,9}$, thus $\tilde{C}_{7,9} = \frac{4\pi}{\alpha_s} C_{7,9}$.

One observes that the real parts are stable, whereas corrections to imaginary parts increase to several percent towards higher q^2 . The effective Wilson coefficients obey the

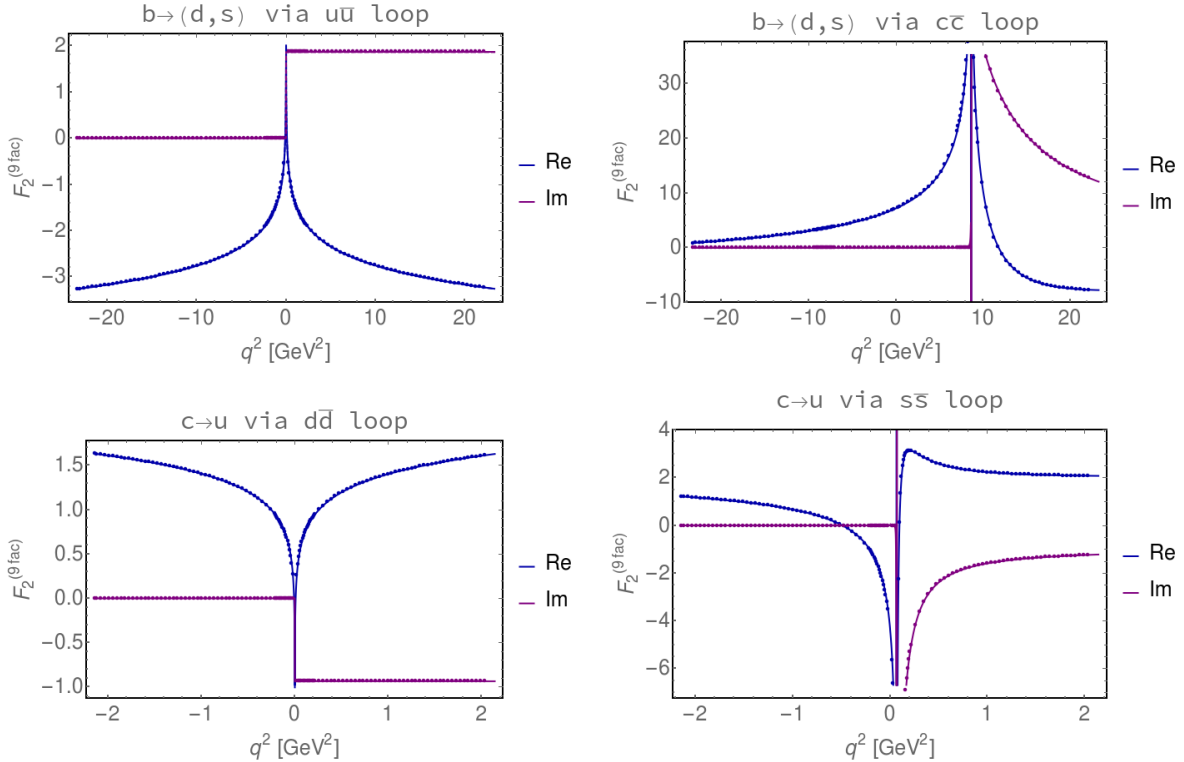


Figure 9: Real (blue) and imaginary (purple) parts of the form factor $F_2^{(9fac)}$ induced by $\langle P_2^{(u)} \rangle$ (upper left), and $\langle P_2^{(c)} \rangle$ (upper right) for $b \rightarrow (d, s)$ transitions and $\langle P_2^{(d)} \rangle$ (lower left), and $\langle P_2^{(s)} \rangle$ (lower right) for $c \rightarrow u$ transitions. The solid lines are fitted to the points, which represent the results of the numerical evaluation. In the lower left plot, the results (three times the function C) of [11] agree with the solid lines.

hierarchies $\text{Re}[\tilde{C}_{7,9}^{\text{eff}}] \gg \text{Im}[\tilde{C}_{7,9}^{\text{eff}}]$. Thus, observables which only depend on the real parts or magnitudes of the effective Wilson coefficients are marginally affected by our results as long as the results of [8, 10, 11] are taken into account. On the other hand, effects on observables which depend on the imaginary parts of the effective Wilson coefficients are significant in the low q^2 range.

Our fitted results of the renormalized form factors $F_2^{(9fac)}$, class 5 in figure 1, are shown in figure 9 for $q^2 \in [-m_h^2, m_h^2]$.

We note that the factorized form factors are smooth below the internal quark pair threshold and real in the Euclidean region. One observes that for vanishing internal masses, see left plots in figure 9, the shapes only differ by the ratio of internal charges and q^2 scales with the ratio of external masses.

4 Summary

In this paper, we calculated the effective Wilson coefficients for heavy to light FCNC transitions induced by the matrix elements of current-current operators at two loop. The results are valid for arbitrary momentum transfer and masses, when the light mass is

neglected. For the MIs, we used the works of [13, 14]. Our computation extends previous works on $b \rightarrow (d, s)\ell^+\ell^-$ transitions [8–11] and is new for $c \rightarrow u\ell^+\ell^-$ transitions. We found significant corrections to the imaginary parts of the effective Wilson coefficients for $b \rightarrow (d, s)$ transitions in the large hadronic recoil range, see figure 8, which should be included in future analyses, including BSM studies. Other corrections for $b \rightarrow (d, s)$ transitions were found to be marginal. For $c \rightarrow u$ transitions and an application to leptoquark models, we refer to [12]. Along with this paper we provide supplemented files, containing our analytical results and fitted results for a specific set of parameters. Finally, our calculation is an independent check of the results of [13, 14] and [8–11], with which we agree in the corresponding limits.

Acknowledgements

We acknowledge Tobias Huber for several useful discussions. We thank Christoph Bobeth and Gudrun Hiller for useful comments on the manuscript. This work has been supported in part by the DFG Research Unit FOR 1873 “Quark Flavour Physics and Effective Field Theories”.

A Supplemented files

The analytical results and the results fitted to points covering the range $|q^2| \leq m_h^2$ for the masses of eq. (23) of the renormalized form factors induced by $\langle \ell\ell | P_{1,2} | h \rangle$ are supplemented to the source files of this paper at <https://arxiv.org/abs/1707.00988>. These supplemented files are described in this appendix and can be used with, e.g., **Mathematica**. Recall that $F_1^{(7)} = \frac{-1}{6}F_2^{(7)}$, $F_1^{(9fac)} = \frac{4}{3}F_2^{(9fac)}$, $F_{1,2}^{(7fac)} = 0$ and that the light external mass is neglected.

The fitted results are provided by the files `fit_F*.dat`, where the asterisk specifies the form factor and the transition, e.g. `fit_F92_btods_ccbar.dat` denotes the form factor $F_2^{(9)}$ for $b \rightarrow (d, s)$ transitions via a $c\bar{c}$ loop (induced by $\langle P_2^{(c)} \rangle$). The fits are functions of polynomials and logarithms in $Q = q^2$ in units of GeV^2 and $MU = \mu^2/m_e^2$, where m_e denotes the (heavy) external quark mass, e.g. $m_e = m_b$ for $b \rightarrow (d, s)$ transitions.

The analytical results are provided by the files `F*.dat`, where the asterisk specifies the form factor and type of polylogarithm, e.g. `F92fac_HPL.dat` denotes the form factor $F_2^{(9fac)}$ in terms of HPLs. The HPL files contain the most general and compact results of this paper, yet individual terms are literally divergent (the full expression is finite). Converted to GPLs, as provided by the `GPL` files, these divergences cancel. Recall that a regularization may be necessary for the numerical evaluation, see section 2.1. Again, $Q = q^2$ and $MU = \mu^2/m_h^2$. Furthermore, `qe` = q_e and `qi` = q_i are the external and internal charges, respectively, `me` = m_e and `mi` = m_i are the external and internal masses. The mass scheme parameter `massscheme` $\rightarrow 0$ for $\overline{\text{MS}}$ masses and `massscheme` $\rightarrow (-4 \ln \frac{\mu^2}{m_i^2} - \frac{16}{3})$ in the pole mass scheme. The arguments of the HPLs are defined by the weight functions as [13]

$$f_{w+}(x) = f_w(x) + f_{-w}(x), \quad f_{w-}(x) = f_w(x) - f_{-w}(x) \quad (24)$$

with

$$w_1 = 1, \quad w_2 = r, \quad w_3 = \frac{r^2 + 1}{2}, \quad w_4 = 1 + \sqrt{1 - r^2}, \quad w_5 = 1 - \sqrt{1 - r^2}. \quad (25)$$

Furthermore,

$$r = \sqrt{1 - 4z_i}, \quad z_i = \frac{m_i^2}{m_e^2} \quad (26)$$

and

$$\begin{aligned} s &= \sqrt{1 - \frac{4z_i}{\bar{u}}}, & s_1 &= \sqrt{1 - \frac{4}{\bar{u}}}, & \bar{u} &= \frac{q^2}{m_e^2}, \\ t &= \frac{1 - s_1}{2} + \frac{1 + s_1}{2} \sqrt{1 + \frac{2(1 - r^2)(1 - s_1)}{(1 + s_1)^2}}, & t_0 &= e^{i\pi/3}r + e^{-i\pi/3}, \\ v &= \frac{1 + s_1}{2} + \frac{1 - s_1}{2} \sqrt{1 + \frac{2(1 - r^2)(1 + s_1)}{(1 - s_1)^2}}, & v_0 &= e^{-i\pi/3}r + e^{i\pi/3}. \end{aligned} \quad (27)$$

Finally, $\mathbf{I} = i$, $\text{Pi} = \pi$, $\text{EulerGamma} = \gamma_E$, $\text{Zeta}[s] = \zeta(s)$, $\text{Sqrt}[z] = \sqrt{z}$, $\text{Log}[z] = \ln(z)$ and $\text{PolyLog}[\mathbf{n}, z] = Li_n(z)$, following the Mathematica notation.

References

- [1] T. Blake et al. “Round table: Flavour anomalies in $b \rightarrow sl^+l^-$ processes”. In: *EPJ Web Conf.* 137 (2017), p. 01001. DOI: 10.1051/epjconf/201713701001. arXiv: 1703.10005 [hep-ph].
- [2] Christoph Greub et al. “The $c \rightarrow u\gamma$ contribution to weak radiative charm decay”. In: *Phys. Lett.* B382 (1996), pp. 415–420. DOI: 10.1016/0370-2693(96)00694-6. arXiv: hep-ph/9603417 [hep-ph].
- [3] Stefan de Boer and Gudrun Hiller. “Flavor and new physics opportunities with rare charm decays into leptons”. In: *Phys. Rev.* D93.7 (2016), p. 074001. DOI: 10.1103/PhysRevD.93.074001. arXiv: 1510.00311 [hep-ph].
- [4] Thorsten Feldmann, Bastian Mueller, and Dirk Seidel. “ $D \rightarrow \rho \ell^+ \ell^-$ Decays in the QCD Factorization Approach”. In: *JHEP* 08 (2017), p. 105. DOI: 10.1007/JHEP08(2017)105. arXiv: 1705.05891 [hep-ph].
- [5] A. Ghinculov et al. “The Rare decay $B \rightarrow X_s l^+ l^-$ to NNLL precision for arbitrary dilepton invariant mass”. In: *Nucl. Phys.* B685 (2004), pp. 351–392. DOI: 10.1016/j.nuclphysb.2004.02.028. arXiv: hep-ph/0312128 [hep-ph].
- [6] Michael Benzke et al. “Factorization at Subleading Power and Irreducible Uncertainties in $\bar{B} \rightarrow X_s \gamma$ Decay”. In: *JHEP* 08 (2010), p. 099. DOI: 10.1007/JHEP08(2010)099. arXiv: 1003.5012 [hep-ph].

- [7] A. Khodjamirian et al. “Charm-loop effect in $B \rightarrow K^{(*)}\ell^+\ell^-$ and $B \rightarrow K^*\gamma$ ”. In: *JHEP* 09 (2010), p. 089. DOI: 10.1007/JHEP09(2010)089. arXiv: 1006.4945 [hep-ph].
- [8] H. H. Asatryan et al. “Calculation of two loop virtual corrections to $b \rightarrow sl^+l^-$ in the standard model”. In: *Phys. Rev. D* 65 (2002), p. 074004. DOI: 10.1103/PhysRevD.65.074004. arXiv: hep-ph/0109140 [hep-ph].
- [9] H. M. Asatrian et al. “Virtual corrections and bremsstrahlung corrections to $b \rightarrow dl^+l^-$ in the standard model”. In: *Phys. Rev. D* 69 (2004), p. 074007. DOI: 10.1103/PhysRevD.69.074007. arXiv: hep-ph/0312063 [hep-ph].
- [10] Christoph Greub, Volker Pilipp, and Christof Schupbach. “Analytic calculation of two-loop QCD corrections to $b \rightarrow sl^+l^-$ in the high q^2 region”. In: *JHEP* 12 (2008), p. 040. DOI: 10.1088/1126-6708/2008/12/040. arXiv: 0810.4077 [hep-ph].
- [11] Dirk Seidel. “Analytic two loop virtual corrections to $b \rightarrow dl^+l^-$ ”. In: *Phys. Rev. D* 70 (2004), p. 094038. DOI: 10.1103/PhysRevD.70.094038. arXiv: hep-ph/0403185 [hep-ph].
- [12] Stefan de Boer. “Probing the standard model with rare charm decays”. <http://hdl.handle.net/2003/36043>. PhD thesis. Technische Universität Dortmund, 2017.
- [13] Guido Bell and Tobias Huber. “Master integrals for the two-loop penguin contribution in non-leptonic B-decays”. In: *JHEP* 12 (2014), p. 129. DOI: 10.1007/JHEP12(2014)129. arXiv: 1410.2804 [hep-ph].
- [14] Hjalte Frellesvig, Damiano Tommasini, and Christopher Wever. “On the reduction of generalized polylogarithms to Li_n and $\text{Li}_{2,2}$ and on the evaluation thereof”. In: *JHEP* 03 (2016), p. 189. DOI: 10.1007/JHEP03(2016)189. arXiv: 1601.02649 [hep-ph].
- [15] J. Kuipers et al. “FORM version 4.0”. In: *Comput. Phys. Commun.* 184 (2013), pp. 1453–1467. DOI: 10.1016/j.cpc.2012.12.028. arXiv: 1203.6543 [cs.SC].
- [16] A. von Manteuffel and C. Studerus. “Reduze 2 - Distributed Feynman Integral Reduction”. In: (2012). arXiv: 1201.4330 [hep-ph].
- [17] S. Laporta. “High precision calculation of multiloop Feynman integrals by difference equations”. In: *Int. J. Mod. Phys. A* 15 (2000), pp. 5087–5159. DOI: 10.1016/S0217-751X(00)00215-7, 10.1142/S0217751X00002157. arXiv: hep-ph/0102033 [hep-ph].
- [18] K. G. Chetyrkin and F. V. Tkachov. “Integration by Parts: The Algorithm to Calculate beta Functions in 4 Loops”. In: *Nucl. Phys. B* 192 (1981), pp. 159–204. DOI: 10.1016/0550-3213(81)90199-1.
- [19] T. Gehrmann and E. Remiddi. “Differential equations for two loop four point functions”. In: *Nucl. Phys. B* 580 (2000), pp. 485–518. DOI: 10.1016/S0550-3213(00)00223-6. arXiv: hep-ph/9912329 [hep-ph].

- [20] R. N. Lee. “Group structure of the integration-by-part identities and its application to the reduction of multiloop integrals”. In: *JHEP* 07 (2008), p. 031. DOI: 10.1088/1126-6708/2008/07/031. arXiv: 0804.3008 [hep-ph].
- [21] Konstantin G. Chetyrkin, Mikolaj Misiak, and Manfred Munz. “ $|\Delta F| = 1$ non-leptonic effective Hamiltonian in a simpler scheme”. In: *Nucl. Phys.* B520 (1998), pp. 279–297. DOI: 10.1016/S0550-3213(98)00131-X. arXiv: hep-ph/9711280 [hep-ph].
- [22] Christoph Bobeth, Mikolaj Misiak, and Jorg Urban. “Photonic penguins at two loops and m_t dependence of $BR[B \rightarrow X_s l^+ l^-]$ ”. In: *Nucl. Phys.* B574 (2000), pp. 291–330. DOI: 10.1016/S0550-3213(00)00007-9. arXiv: hep-ph/9910220 [hep-ph].
- [23] Jens Vollinga and Stefan Weinzierl. “Numerical evaluation of multiple polylogarithms”. In: *Comput. Phys. Commun.* 167 (2005), p. 177. DOI: 10.1016/j.cpc.2004.12.009. arXiv: hep-ph/0410259 [hep-ph].
- [24] Sebastian Kirchner. “LiSK - A C++ Library for Evaluating Classical Polylogarithms and Li_{22} ”. In: (2016). arXiv: 1605.09571 [hep-ph].
- [25] Daniel Maitre. “Extension of HPL to complex arguments”. In: *Comput. Phys. Commun.* 183 (2012), p. 846. DOI: 10.1016/j.cpc.2011.11.015. arXiv: hep-ph/0703052 [hep-ph].
- [26] Tobias Huber and Daniel Maitre. “HypExp 2, Expanding Hypergeometric Functions about Half-Integer Parameters”. In: *Comput. Phys. Commun.* 178 (2008), pp. 755–776. DOI: 10.1016/j.cpc.2007.12.008. arXiv: 0708.2443 [hep-ph].